Short grafted chains: Monte Carlo simulations of a model for monolayers of amphiphiles

Christoph Stadler, Harald Lange, Friederike Schmid
Institut für Physik, Universität Mainz, D-55099 Mainz, Germany

Abstract. We present Monte Carlo simulations of a coarse-grained model for Langmuir monolayers of amphiphile molecules on a polar substrate. The molecules are modelled as chains of Lennard-Jones beads, with one slightly larger end bead confined in a planar surface. They are simulated in continuous space under conditions of constant pressure, using a simulation box of variable size and shape. The model exhibits a disordered phase (corresponding to the liquid expanded phase), and various ordered phases (corresponding to the condensed phases) with different types of tilt. We calculate the phase diagrams and characterize the different phases and phase transitions. The effect of varying the chain stiffness is also discussed.

I. INTRODUCTION

Monolayers of amphiphiles at surfaces (Langmuir monolayers) have attracted longstanding scientific interest for various reasons [1–3]: Surface properties of materials can be modified and taylored by coating the surfaces with amphiphiles. Langmuir monolayers can be exploited to engineer thin film materials with well-defined structures on a molecular level. On the other hand, lipid monolayers on water are experimentally fairly accessible model systems for biological membranes. Last not least, Langmuir monolayers are experimental realizations of two-dimensional systems, which allow to study ordering phenomena in low dimensions.

Experimentally, Langmuir monolayers have been investigated for a long time by measurements of pressure-area isotherms [1]. More recently, a number of powerful microscopy techniques have been developed, such as fluorescence microscopy and Brewster angle microscopy, which have provided insight into the mesoscopic structures in monolayers. The emerging pictures for monolayers on water is qualitatively similar for phospholipids, long chain alcohols and esters: At low surface coverage, the molecules hardly interact with each other and build the two-dimensional equivalent of a "gas". Upon compression, a first order transition to a fluid-like "liquid expanded" (LE) phase is encountered, followed at even higher surface coverage by a second discontinuous transition into a "liquid condensed"(LC) area. The transition from liquid expanded to liquid condensed has an important equivalent in bilayers, the "main transition", which may be biologically relevant, since it takes place at temperatures close to the body temperature for some of the common phospholipids. The condensed region contains a variety of different phases, characterized by different types of

ordering, *i.e.*, collective tilt order of the hydrocarbon chains, orientational order of the backbones of the chains, and crystalline positional order. A generic phase diagram for fatty acid monolayers is shown in Fig. 1 [3]. The lowest density phases which coexist with the LE phase are typically hexatic rotator phases, *i.e.*, the backbones rotate freely around, and positional correlations decay exponentially, but the directions of nearest neighbors are nevertheless well-defined.

Theoretical treatments of Langmuir monolayers have followed three different lines. On the one hand, phenomenological descriptions of the different condensed phases in terms of Landau expansions in the characteristic order parameters [4,5] have offered valuable insight into the nature and the interrelations of different phase transitions on a very general level. On the other hand, Molecular dynamics simulations of atomically realistic models have complemented experiments and provided structural information on quantities, which are hard to access experimentally [7–11]. These two approaches are in a sense antipodal: Whereas phenomenological treatments focus on universal properties and make little or no contact to the microscopic structure of the systems, atomically realistic models seek to imitate nature as faithfully as possible, and to reach quantitative agreement. Hence they account for many more details than are actually needed to produce a certain phase behavior, rely heavily on the availability of good force fields, and their study is computationally costly.

As a third line of approach, idealized microscopic models are constructed which incorporate only a few properties of a material, believed to be essential for a given behavior. Thus they bridge between phenomenological and realistic models, and relate microscopic and macroscopic quantities in a qualitative and semi-quantitative way.

The question, which features of amphiphiles are essential in Langmuir monolayers, can of course not be answered universally. It depends on the region in phase space one wishes to study. Attractive interactions between the amphiphiles are important for most phase transitions. As long as one studies condensed phases, it is often sufficient to model the amphiphiles as anisotropic stiff objects. Grafted rigid rods exhibit tilt transitions [12–14], molecules with non-circular cross-sections show rotator transitions [15]. For the transition between the liquid condensed and the liquid expanded phase, however, the conformational degrees of freedom of the chains play a crucial role [10,16,17]. They have been incorporated in a heuristic way as "internal degeneracies" in Ising-type two-dimensional lattice models for monolayers and bilayers, *e.g.*, in the Pink model [18,19]. The interdependence of chain conformations and effective chain interactions has to be put in by hand in this approach, and a large number of input parameters is required. Models which aim to study more directly the interplay of chain conformations and phase behavior have to retain the chain character of the amphiphiles explicitly.

A suitable idealized model for Langmuir monolayers thus represents the amphiphiles by flexible chains of mutually attracting monomers, which are grafted to a surface at one end ("head"). Such models have been formulated on the lattice [20–24] and in continuous space [25–29].

Lattice models can be simulated more efficiently than off-lattice models, yet they can produce rather awkward lattice effects especially when orientational order (tilt order) comes into play [24]. An off-lattice bead-spring model of Lennard-Jones beads has been studied by Haas *et al* [25,26] and by us [27] under constant volume and constant pressure conditions. It was found to display a tilted and an untilted phase, in which the chains are basically arranged on a (possibly distorted) hexagonal lattice, and a "fluidized" phase which is reminiscent of

the liquid expanded phase. Hence it seems a promising candidate for a minimal model, which contains only the basic elements responsible for the main transition in Langmuir monolayers. Nevertheless, no systematic study of the phase behavior has been presented so far.

This is the objective of the present paper. We have performed Monte Carlo simulations of a bead-spring model very similar to the one used by Haas *et al*. The models only differ in the treatment of the heads: Whereas the head beads in Haas *et al*'s version are identical with the chain beads, our heads are slightly larger. We chose this variant in order to ensure that the dominant reason for chain tilting in our model is similar to the most common one in nature: Tilt is induced by the mismatch of head and tail size. In the model of Haas *et al*, the chains tilt, because they can then "hook" into each other and thus pack more efficiently. The details of the tilt order (tilt angle, tilt direction etc.) result from a complicated interplay between monomer packing and chain stretching [26], which is highly model dependent and has probably little to do with the factors which influence the tilt in real monolayers. On simple geometrical grounds, two of us have argued earlier that the direction of tilt depends on the size of the head groups [30]. There is also experimental evidence for such a connection [31]. With our choice of the head size, we ensure that the model exhibits two different tilted phases at zero temperature, a low-pressure one with tilt towards nearest neighbors, and a higher-pressure one with tilt towards next nearest neighbors.

Our paper is organized as follows: In the next section, we specify the model and comment on some aspects of the simulation techniques and the data analysis. The results are presented in section 3: We characterize the phases and phase transitions, show the phase diagrams, and discuss the effect of the chain stiffness. We summarize and conclude in section 4.

II. MODEL AND TECHNICAL DETAILS

Following Haas *et al* [25,26], we model the amphiphiles as chains of beads, which are connected by springs of length d subject to the spring potential

$$V_S(d) = \begin{cases} -\frac{k_S}{2} {d_S}^2 \ln\left(1 - (d-d_0)^2/{d_S}^2\right) & \text{for } |d-d_0| < d_S \\ \infty & \text{for } |d-d_0| > d_S \end{cases} \tag{1}$$

This so-called "Finite extension nonlinear elastic" potential (FENE) is basically harmonic at $d \approx d_0$ and has a logarithmic cutoff at $d = d_0 \pm d_S$. Furthermore, we impose a stiffness potential

$$V_A = k_A \cdot (1 - \cos\theta) \tag{2}$$

on the angle θ between subsequent springs. The stiffness potential favors angles $\theta = 0$, *i.e.*, straight chains. Beads are not allowed to enter the half space $z < 0$; moreover, one end bead of each chain (the "head") is confined to remain within the plane $z = 0$. Thus we assume a very strong binding force between the hydrophilic head group and the water surface, and the latter is approximated by a perfectly sharp and flat interface. Tail beads interact *via* a truncated Lennard-Jones potential

$$V_{LJ}(r) = \begin{cases} \epsilon \cdot \left((\sigma/r)^{12} - 2(\sigma/r)^6 + v_c \right) & \text{for } r \le 2\sigma \\ 0 & \text{for } r > 2\sigma \end{cases}, \tag{3}$$

where $v_c = 127/4096 \approx 0.031$ is chosen such that $V_{LJ}(r)$ is continuous at $r = 2\sigma$. The interactions between head beads are purely repulsive,

$$V_H(r) = \begin{cases} \epsilon_H \cdot \left((\sigma_H/r)^{12} - 2(\sigma_H/r)^6 + 1 \right) & \text{for } r \le \sigma_H \\ 0 & \text{for } r > \sigma_H \end{cases}. \tag{4}$$

The attractive part here has been cut off for reasons of computational efficiency. Note that the head size σ_H differs from the tail bead size σ. Head and tail beads interact with a repulsive potential of the form (4), in which σ_H is replaced by $(\sigma_H + \sigma)/2$.

The parameters ϵ and σ define the units of energy and length. To complete the definition of the model, we have to specify the remaining parameters d_0, d_S, k_S, k_A, ϵ_H, and σ_H: Our choice was motivated by the idea that one bead should represent roughly two CH_2 groups in an actual alkane chain. Comparing a straight model chain with an ideal all-trans state hydrocarbon chain, with realistic potential parameters of united-atom potentials taken from the literature (*e.g.*, from Ref. [32]), one finds that the bond length d_0 should be approximately 0.7 times the chain diameter, $d_0 = 0.7\sigma$. The identification also allows for a rough estimate of the absolute values of σ and ϵ: $\sigma \approx 3.8\mathring{A}$ and $\epsilon \approx 240 k_B K$, where k_B is the Boltzmann constant. These values should of course not be taken too literally, since the model is much too simple to allow for quantitative comparisons with experimental systems.

The spring constant k_S was chosen very strong, $k_S = 100\epsilon$, such that the lengths of the springs are approximately constant at all temperatures of interest. The value of the cutoff d_S then has little influence on the properties of the system; we use $d_S = 0.2\sigma$. The stiffness constant k_A can be estimated by adjusting the average $\langle \cos\theta \rangle$ of a single free chain in our model at a given temperature to the corresponding value in a single free alkane chain. Such an estimate would yield $k_A \approx 5\epsilon$ at room temperature. Haas *et al* [25,26] have used $k_A = 10\epsilon$. Here, we have mostly used the same value ($k_A = 10\epsilon$) in order to be consistent with their work. For the reasons mentioned in the introduction, the size of the head beads was taken to be $\sigma_H = 1.1\sigma$. The influence of the head size on the phase behavior shall be discussed in detail elsewhere [29,33]. The prefactor ϵ_H was chosen $\epsilon_H = \epsilon$.

The simulations were performed at constant spreading pressure in a simulation box of variable size and shape. More specifically, we study n chains of length N on a parallelogram with side length L_x and L_y and angle α. Periodic boundary conditions were applied in these two directions, and free boundary conditions in the third. Our Monte Carlo moves include:

- Attempts to displace single beads
- Attempts to vary L_x, L_y or α, *i.e.*, to rescale all coordinates such the the configuration is stretched or squeezed in one direction, or sheared ("volume moves")

The trial moves are accepted or rejected according to a standard Metropolis prescription with the effective Hamiltonian [34]

$$H = E + \Pi A - nNT \ln(A), \tag{5}$$

where E is the internal energy, Π the applied spreading pressure, and $A = L_x L_y \sin\alpha$ the area of the simulation box. We have also implemented collective moves, in which chains were displaced as a whole, and volume moves, in which only the coordinates of the head beads are rescaled, but inner molecular distances and angles are kept constant. The Hamiltonian (5) then has to be replaced by

$$H = E + \Pi A - nT \ln(A). \tag{6}$$

Unfortunately, these collective moves did not reduce the time needed to generate uncorrelated configurations significantly. Similarly, we have implemented continuous configurational biased Monte Carlo moves [35], but found that they brought no improvement in our particular system.

In order to check that no internal stress is present in our simulations, we have determined the internal pressure tensor

$$\Pi^{int}_{\alpha\beta} = \frac{1}{A}\langle \sum_{i=1}^{nN} r_{i\alpha} F_{i\beta} \rangle + \frac{N k_B T}{A} \delta_{\alpha\beta}, \tag{7}$$

where the sum i runs over all monomers, α, β over the x and y coordinate, $\vec{F}_i$ denotes the force acting on monomer i, and $\delta_{\alpha\beta}$ is the unit matrix. According to the virial theorem, $\Pi^{int}_{\alpha\beta}$ should be diagonal and identical to $\Pi\delta_{\alpha\beta}$ at mechanical equilibrium. This was the case in our simulations, if we used a simulation box of variable shape. In simulation runs with a rectangular box, we sometimes obtained nonzero off-diagonal elements Π_{xy} in the tilted phases.

We will present results for $n = 144$ chains of length $N = 7$. The average decorrelation time lies between 200 and 1000 Monte Carlo steps (MCS), where one MCS consists of $Nn = 1008$ attempts of monomer moves, and one attempt to rescale L_x, L_y, and α. In general, the systems were equilibrated during 70.000 MCS, and data were then collected from every 500st configuration over a period of at least 200.000 MCS.

The simulations were supplemented by a low temperature analysis. The zero temperature ground state was determined by minimization of the enthalpy (5). A harmonic expansion was then performed in order to determine the free energy G at some given low (nonzero) temperature T_0. Given this reference value, one can calculate the free energy at other temperatures and pressures from simulations by means of a thermodynamic integration

$$G(\Pi, T) = G(\Pi_0, T_0) + k_B T \int_\Gamma \Big\{ d\Pi' \frac{A}{k_B T'} - dT' \frac{H}{k_B T'^2} \Big\}, \tag{8}$$

as long as the path Γ from (Π_0, T_0) to (Π, T) does not cross a first order phase transition. By comparing the free energies of different states, we have localized the transition points between phases at low temperatures where hysteresis effects were strong.

III. RESULTS

Figure 2 shows temperature-area isobars for a selection of low pressures (a) and high pressures (b). One clearly observes a jump in the area per molecule, which moves to higher

temperatures as the pressure increases. At high pressures, one discernes in addition a kink at low temperatures, indicating the presence of a second phase transition.

The phases can be characterized by the typical features of the pair correlation functions (Figs. 3 and 4) and structure functions (Figs. 5 and 6). For example, the two dimensional correlation functions in the intermediate temperature state at high pressures are precisely those of a hexagonal lattice. Fig. 3 shows pair correlation functions for the head groups, the projection of center of gravity of the chains onto the xy plane, and the points where the chains pass through the plane at $z = 2\sigma$ above the surface at pressure $\Pi = 100\epsilon/\sigma^2$ and temperature $T = 1\epsilon/k_B$, which is slightly above the first phase transition. The three curves do not differ from each other qualitatively, and the position and relative heights of the peaks are consistent with those of a hexagonal structure. At temperatures below the first phase transition or at lower pressures, each of the peaks splits up in two. This indicates that the hexagonal lattice is distorted in one of the high symmetry directions, either the nearest neighbor or the next nearest neighbor direction (for intermediate directions the peaks would split up in three). An example is shown in Fig. 4 (see the curves for the lowest temperature $T = 0.1\epsilon/k_B$). From the large height difference of the twin peaks, one can infer that the lattice is stretched in the direction of nearest neighbors in this specific case. The direct inspection of configuration snapshots reveals, not surprisingly, that the lattice distortion goes along with a collective tilt of the chains in the direction of the distortion. At low pressures ($\Pi \lesssim 10\epsilon/\sigma^2$), the hexagonal lattice in the tilted phases is stretched by roughly 10 %.

With increasing temperature, the structure of the correlation functions is gradually lost. Slightly below the phase transition, the correlation functions of the head lattice are fluid-like, with peaks of monotonically decreasing height for the first, second and third coordination shell. They do not change qualitatively as the phase transition is crossed (Fig. 4 (a)). In contrast, the correlation function for the projections of the center of gravity still shows some solid-like structure right below the phase transition, and loses almost every structure right above the phase transition (Fig. 4 (b)). In the high temperature state, the head positions are much more correlated than the chain positions. We conclude that the phase transition associated to the area jump is a melting transition, and that it is driven by the chains. The chains maintain the order below the transition, and promote the disorder above the transition. This is consistent with results from molecular dynamics simulation by Karaborni and Toxvaerd [11] of a realistic model.

The structure function is defined by

$$S(\vec{q}) = \frac{1}{nN}\left|\sum_{j=1}^{nN}\exp(i\vec{q}\vec{r}_j)\right|^2, \tag{9}$$

where the sum runs over all monomers in the system. Note that in a finite simulation box with periodic boundary conditions, $S(\vec{q})$ for a specific configuration is only defined for vectors $\vec{q}$ whose projection on the xy plane are sums of integer multiples of the basis vectors

$$\vec{b}_x = \frac{2\pi}{L_x}\begin{pmatrix}1\\ -1/\tan(\alpha)\end{pmatrix} \qquad \text{and} \qquad \vec{b}_y = \frac{2\pi}{L_y}\begin{pmatrix}0\\ 1/\sin(\alpha)\end{pmatrix}.$$

However, the dimensions of the box fluctuate in our simulations, hence the basis vectors fluctuate as well. In order to overcome this problem, we have laid a fine-meshed grid on the

xy plane and summed up all the contributions to $S(\vec{q})$ within a mesh. Fig. 5 (a) and (b) shows the resulting structure factors in the plane of $q_z = 0$ for an disordered state (a) and an untilted ordered state (b). The structure factor of the disordered state is isotropic and shows the usual features of a fluid structure factor. In the untilted ordered state, one finds the Bragg rods of the hexagonal lattice. They are sharply peaked in the xy plane, but have a considerable width in the z direction, thus the term "rods". In the tilted ordered state, the plane of maxima tilts such that it stays perpendicular to the long axis of the chains [3]. Thus the peaks belonging to $\vec{q}$ vectors which are not perpendicular to the tilt direction move out of the $q_z = 0$ plane. This is illustrated in Fig 6 for a state with tilt towards next nearest neighbors. The internal structure of the rods in the z-direction reflects the structure of the monolayer. For example, the width of the rods is inversely proportional to the width of the layer, and every rod is surrounded by a multitude of weak "satellite maxima" which are caused by the sharp steps in the density profile at $z = 0$ and at the outer surface. After six low satellite maxima, another strong peak is found, reaching a height comparable to that of the main peak. These peaks reflect the "periodic" arrangement of monomers *within* a chain. They are found at distances of approximately $\Delta q_z \approx 2\pi/d_0 \cos\theta$ and integer multiples from the main peak, where d_0 is the favored distance between monomers (see eqn. (1)). Their appearance is a very specific property of our simulation model, and not interesting from a general point of view. Hence they shall not be studied any further.

In order to quantify our findings, we have analyzed a number of suitable order parameters. For example, we determine the hexagonal order parameter of two dimensional melting

$$\Psi_6 = \left\langle \left| \frac{1}{6n} \sum_{j=1}^{n} \sum_{k=1}^{6} \exp(i6\phi_{jk}) \right|^2 \right\rangle. \tag{10}$$

Here the first sum j runs over all heads of the systems, the second k over the six nearest neighbors of j, and ϕ_{jk} is the angle between the vector connecting the two heads and an arbitrary reference axis. The quantity Ψ_6 thus measures the orientational long range order of nearest neighbor directions. It is nonzero in the hexagonal (quasi)crystalline phase and in the hexatic phase. As an order parameter which describes the collective tilt of molecules, we have computed

$$R_{xy} = \sqrt{\langle [x]^2 + [y]^2 \rangle}, \tag{11}$$

which corresponds to the length of the average projection of the head-to-end vector of the chains on the xy plane. Here $[x]$ and $[y]$ denote the x and y component of the head-to-end vector, averaged over the chains of a configuration, and $\langle \cdot \rangle$ denotes the thermal average over all configurations. The quantitity R_{xy} is nonzero in phases which break the azimuthal symmetry, *i.e.*. phases with collective tilt, and zero otherwise. Note that the average tilt angle θ between the head-to-end vector of the chains and the surface normal is always nonzero.

The quantities Ψ_6 and R_{xy} are shown as a function of temperature for various pressures in Figs. 7 and 8. The area jump in the isobars goes along with a drop to almost zero of the melting order parameter Ψ_6. This substantiates our earlier speculation that the transition corresponds to a melting transition. Furthermore, we infer from the decrease of R_{xy} with the temperature, that there is also a tilting transition from a collectively tilted phase at small temperatures, to an untilted phase at high temperature. The melting transition and

the tilting transition occur simultaneously at low pressures, and decouple from each other at high pressures. The tilting transition then precedes the melting transition and seems to be continuous.

At our small system size, it is not possible to decide whether the ordered phase is crystalline or hexatic. Moreover, we are not able to establish unambiguously the order of the melting transition. These are two closely related issues of high interest. Even in much simpler two dimensional systems (hard disks, Lennard-Jones disks), the question whether they melt discontinuously in one stage, or continuously *via* a hexatic phase [36] in two stages, is still a matter of debate. The transition from a hexatic to a fluid phase is usually believed to be continuous. In the case of amphiphile monolayers, however, we have argued that it can be driven first order, as an effect of the interplay between chain entropy and chain packing [17]. We have already noted that the melting transition in our system is mainly driven by the chains, which enhances the likelihood of such a scenario. The transition may also be discontinuous at low and intermediate pressures, and continuous at high pressures. The pronounced jumps observed in our simulations seem to indicate a line of discontinuous transitions; on the other hand, we have not encountered significant hysteresis effects except at very low pressure, $\Pi = 1$. Simulations of much larger systems and a thorough finite-size analysis would presumably be necessary to distinguish between first order and continuous transitions.

It is instructive to also consider the distribution of tilt angles θ. Let us first look at the average $\langle\theta\rangle$ (Fig. 9). In the low pressure regime, where the melting and the tilting phase transition coincide, it drops down at the transition and then rises slowly with temperature. At higher pressures, where the two transitions decouple, it first decreases with temperature until the tilting transition is passed, then stays low in the temperature region of the untilted ordered phase, but jumps to a higher value at the melting transition. The jump is related to the jump in the area per molecule at that transition: the molecules have more space to lie down. The average tilt angle is coupled to the molecular area A/n by the requirement that the bead density in the monolayer should not vary much, i.e., the total volume occupied by the monolayer is close to constant. In the condensed region, where the chains are mostly straight and aligned, this implies that the quantity $A\cos(\theta)/n$ is approximately constant and equal to a_c, the area per molecule in the untilted high pressure phase. Such a dependence has indeed been reported experimentally [37]. Similarly, we find here that the product of A and $\cos(\langle\theta\rangle)$ depends much less on the temperature and pressure than the area per molecule A/n itself (Figure 10). In particular, its value right below the melting transition is found to be $a_c \sim 0.985\sigma^2$ at all pressures except for the very highest, $\Pi = 100\epsilon/\sigma^2$, regardless of whether the condensed phase is tilted or untilted. Hence the *volume* density in the monolayer seems to trigger the melting transition rather than the area density – which corroborates our earlier assertion that the melting transition is driven by the chains.

Figure 11 shows the histogram of the tilt angle $P(\theta)/\sin\theta$ at pressure $\Pi = 50$ for different temperatures. Below the tilting transition, $P(\theta)/\sin\theta$ has a clear maximum. As the temperature is increased, the maximum moves down towards lower values θ. At the tilting transition, it merges into $\theta = 0$. From there on, it becomes broader, which explains the increase of $\langle\theta\rangle$ at higher temperatures.

Finally, we turn to the discussion of the direction of the tilt. It can be determined from a histogram of the angle between the momentary tilt direction and the bonds connecting nearest neighbors. If the tilt angle is well-defined, this histogram should have six peaks, and

their positions indicate the direction of tilt. At low temperatures $T \lesssim 0.1$, we find two phases with well-defined tilt directions towards nearest neighbors and next nearest neighbors. The transition between them is strongly first order, and the thermodynamic integration methods described in the previous section had to be used to locate the transition points. At higher temperatures, the transition washes out, and in some regions of phase space it is hard to determine whether the tilt direction is at all locked to the underlying hexagonal head lattice. In order to quantify the "locking", we define an order parameter Φ_6, which is very similar to the hexagonal order parameter Ψ_6 (eqn. (10)).

$$\Phi_6 = \left| \left\langle \frac{1}{6n} \sum_{j=1}^{n} \sum_{k=1}^{6} \exp(i6\phi'_{jk}) \right\rangle \right|^2. \tag{12}$$

The notation corresponds to that in eqn. (10), except that ϕ'_{jk} is now the angle to the average tilt direction in the current configuration rather than simply that to an arbitrary reference axis. The crucial difference to the definition of ψ_6 lies in the detail that the sequence of $\langle . \rangle$ and $|.|$ has been interchanged. The parameter Φ_6 is nonzero if the tilt direction is locked to the nearest neighbor, next nearest neighbor, or to an intermediate direction. However, it would still be zero in a special case of locked state, where the tilt jumps between nearest and next nearest neighbors. In order to distinguish such a state from one where the tilt direction is really oblivious to the hexagonal lattice, we have also evaluated the related parameter Φ_{12}

$$\Phi_{12} = \left| \left\langle \frac{1}{6n} \sum_{j=1}^{n} \sum_{k=1}^{6} \exp(i12\phi'_{jk}) \right\rangle \right|^2. \tag{13}$$

The parameter Φ_6 and Φ_{12} are shown in Fig. 12 for fixed temperature $T = 0.5\epsilon/k_B$ as a function of pressure. At this temperature, the monolayer is tilted at all pressures shown. Fig. 7 demonstrates that the tilt direction is locked to the hexagonal lattice at low pressures, but apparently unlocks at $\Pi = 40\epsilon/\sigma^2$. That unlocked phases should exist in tilted *hexatic* liquid crystal films has been claimed by Selinger and Nelson [6]. In crystalline phases, they are supposedly suppressed by the elastic interactions. Since our systems are too small to allow for a distinction between hexatic and crystalline order, they are obviously also too small to allow to decide whether the unlocked state is real or a finite-size artefact.

In order to study the role of the chain flexibility, we have also performed a few shorter simulation runs (35.000 MCS) of systems with stiffer chains [28]. To this end, the stiffness constant k_A (cf. eqn. (2)) was increased by a factor of ten, $k_A = 100\epsilon$. The area per molecule A/n, the melting order parameter Ψ_6 and the order parameter of collective tilt R_{xy} for these systems are shown as a function of temperature for three different pressures $\Pi = 10, 30$ and $40\epsilon/\sigma^2$ in Fig. 13. Up to the highest pressure $\Pi = 40\epsilon/\sigma^2$, the melting transition and the tilting transition are coupled. Moreover, the melting transition is shifted to much higher temperatures. This demonstrates once more that the melting transition in the system is basically driven by the chains.

Our results for flexible chains are summarized in the phase diagrams Fig. 14 and Fig. 15. We find at least four phases: the disordered fluid, an untilted ordered phase, two tilted ordered phases with tilt towards nearest neighbors and next nearest neighbors, and possibly an unlocked tilted phase. The areas per molecule of the two locked tilted phases are almost equal at the transition, even at low temperatures where the latter is strongly first order. At higher temperatures, the transition is so washed out that it cannot be located any more.

The transition between the tilted and the untilted ordered phase seems continuous. Between the tilted ordered phase and the disordered phase, it is presumably first order. The order of the transition between the untilted ordered phase and the disordered phase could not be determined, as discussed above. It should be stressed that none of our assertions on the order of the transitions has been corroborated by a finite size analysis, hence they should be regarded with caution.

At surface areas per molecules smaller than $A \approx 0.8\sigma^2$, *i.e.*, at high pressures and low temperatures, the chains are squeezed together so closely that they form "rippled" structures where the beads of chains in neighbor rows are displaced with respect to each other in the z direction. This effect is clearly an artefact of our model and has not been investigated in detail, nor included in the phase diagram Fig. 13. In the limit of vanishing pressure, on the other hand, the system has to assume a gas phase at all temperatures for entropic reasons. The transition between the gas phase and the condensed phase is subject to strong hysteresis effects at low temperatures. Nevertheless, we have been able to determine the area per molecule of the coexisting condensed state without too much computational effort on the basis of the following consideration: An upper limit is given by the area per molecule of the metastable condensed state at zero pressure, which does not decay within the simulation time at temperatures below $T = 1.35\epsilon/k_B$. A lower limit is provided by the area per molecule at the smallest pressure for which the transition temperature from the ordered to the disordered state has been determined, in our case $\Pi = 1\epsilon/\sigma^2$. Since the areas per molecule do not depend strongly on the pressure in the condensed state, the coexistence line can thus be located fairly accurately (see Fig. 14).

Within the region of the disordered fluid, we have not found evidence for an additional liquid/gas transition. Such a transition would be expected at areas per molecule much larger than $\sim 3\sigma^2$ (where the critical point is found in two dimensional Lennard-Jones fluids [38]), and correspondingly low surface pressures. We have spent some time searching for it, varying the temperature at very low pressure $\Pi = 0.05\epsilon/\sigma^2$, and driving the pressure to zero at the temperature $T = 1.45\epsilon/k_B$ [39]. In a region around ($\Pi = 0.05\epsilon/\sigma^2, T \approx 1.7\epsilon/k_B$) or ($\Pi \approx 0.04\epsilon/\sigma^2, T = 1.45\epsilon/k_B$), the area per molecule varied rapidly, and strong density fluctuations were encountered. This suggests that liquid-gas critical point may be nearby. However, we have not been able to locate it so far. It may be hidden in the coexistence region.

IV. CONCLUSIONS

To summarize, we have studied in detail the phase behavior of a model of grafted Lennard-Jones chains, which is of interest as a "minimal" model for amphiphile monolayers. The model was found to show an impressive variety of phases, and its analysis gives useful insight into the mechanisms which drive some of the phase transitions in amphiphilic layers. In particular, it exhibits a disordered phase, an untilted ordered phase, and a number of tilted ordered phases, which are also found experimentally in Langmuir monolayers. The sequence of tilting transitions with increasing pressure (tilt towards nearest neighbors, tilt towards next nearest neighbors, no tilt) agrees with experiments and with earlier theoretical predictions. Furthermore, we have discussed the transition to the fluid state, and concluded from the form of the pair correlation functions in the different phases, and from the way the

transition temperature depends on the chain stiffness, that the transition is mainly driven by the chains, again in agreement with experimental [16] and theoretical [10,11,17] observations.

In other respect, the phase diagram is still quite different from the experimental one (Fig. 1). Some of the discrepancies are not surprising; for example, the model with its rotationally symmetric chains was never designed to reproduce the herringbone-ordered low-temperature structures. Other differences are more interesting. The pressure at the transition from the tilted to the untilted phase decreases strongly with temperature, whereas it is almost independent of the temperature in experimental systems. Likewise, the transition pressure of the swiveling transition between nearest neighbor tilt and next nearest neighbor tilt increases with temperature, whereas the line separating the Ov and L_2 phase in Fig. 1 moves to lower pressures. This is presumably a consequence of the treatment of the head groups – more specifically, of the rigid constraints which are imposed on them in the model. The hard core interactions are much harder than the effective interactions between real head groups in water. Moreover, the heads in our model are confined to lie in a plane, whereas they can move in and out of the surface in real systems [40].

Further refinements of the model will thus have to focus on the representation of the head groups. We have already mentioned the interplay between head size, spreading pressure, and tilting transitions. A more detailed study of the influence of the head size on the phase behavior shall be presented elsewhere [33]. Future work will be concerned with the effect of relaxing some of the constraints on the head groups, *i.e.*, giving them additional degrees of freedom in the z-direction, and possibly softening the interactions between them. One could also think of introducing interactions between the tails and the substrate. However, the tails hardly come into contact with the substrate at most densities of interest, therefore this will probably not change the phase behavior significantly.

On the other hand, we have seen that already the present simple model reproduces many important properties of amphiphile monolayers. Hence it can be used as a starting point for further investigations. In particular, simulations of much larger systems and a systematic variation of system sizes would be desirable to shed light on some of the questions which have remained open in the present study. These would help to elucidate the exact nature of the tilting transitions and the order of the melting transition, to examine the unlocked tilted state, and to clarify whether our model actually does exhibit hexatic phases.

ACKNOWLEDGMENTS

We are grateful to Kurt Binder for numerous enlightening discussions, and to Frank Martin Haas and Rudolf Hilfer for sharing with us their expertise on the simulation of these systems, and in particular for letting us have their simulation code, which has been an invaluable starting point for the development of our own. We have benefitted from useful interactions with Burkhard Dünweg, Peter Nielaba, and Nigel Wilding. F.S. is supported by the Deutsche Forschungsgemeinschaft through a Heisenberg fellowship, and C.S. through a Ph.D. studentship associated with the Graduiertenkolleg on supramolecular systems in Mainz.

[1] G. M. Bell, L. L. Combs, L. J. Dunne, Chem. Rev. **81**, 15 (1981); H. Möhwald, Ann. Rev. Phys. Chem. **41**, 441 (1990); H. M. McConnell, ibid **42**, 171 (1991); C. M. Knobler, R.C. Desai, ibid **43**, 207 (1992). D. Andelman, F. Brochard, C.M. Knobler, F. Rondelez, in *Micelles, Membranes, Microemulsions and Monolayers*, p. 559, W. M. Gelbart, D. Roux and A. Ben-Shaul eds. (Springer, 994).

[2] W. A. Barlow, *Langmuir-Blodgett Films* (Elsevier, 1980); M. C. Petty, *Langmuir-Blodgett Films* (Cambridge University Press, 1996).

[3] V. M. Kaganer, H. Möhwald, P. Dutta, Rev. Mod. Phys., in press (1998).

[4] J.V. Selinger, Z. Wang, R.F. Bruinsma, C.M. Knobler, Phys. Rev. Lett. **70**, 1139 (1993);

[5] V. M. Kaganer, E. B. Loginov, Phys. Rev. Lett. **71**, 2599 (1993); Phys. Rev. E **51**, 2237 (1995); V. M. Kaganer, V. L. Indenbom, J. Phys. II France **3**, 813 (1993).

[6] J. V. Selinger, D. R. Nelson, Phys. Rev. A **39**, 3135 (1989).

[7] A. J. Kox, Nature **285**, 317 (1980); S. H. Northrup, M. S. Curvin, J. Phys. Chem. **89**, 4707 (1985). M. A. Moller, D. J. Tildesley, K. S. Kim, N. Quirke, J. Chem. Phys. **94** 8390 (1991). P. Ahlström, J. C. Berendsen, J. Phys. Chem. *97* 13691 (1992).

[8] J. P. Bareman, G. Cardini, M. L. Klein. Phys. Rev. Lett. **60**, 2152 (1988). G. Cardini, J. P. Bareman, M. L. Klein. Chem. Phys. Lett. **145**, 493 (1988); J. P. Bareman, M. L. Klein. J. Phys. Chem. **94**, 5202 (1990). J. Hautman, M. L. Klein, J. Chem. Phys. **91**, 4994 (1989); **93**, 7483 (1990).

[9] H. E. Alper, D. Bassolino, T. R. Stouch. J. Chem. Phys. **98**, 9798 (1993); **99**, 5547 (1993).

[10] J. Harris, S. A. Rice, J. Chem. Phys. *89*, 5898 (1988). S. Shin, N. Collazo, S.A. Rice, J. Chem. Phys. **96**, 1352 (1991); **98**, 3469 (1992); N. Collazo, S. Shin, S.A. Rice, J. Chem. Phys. **96**, 4735 (1991); J. Gao, S. A. Rice, J. Chem. Phys. **99**, 7020 (1993); M. E. Schmidt, S. Shin, S. A. Rice, J. Chem. phys. **104** 2101 and 2114 (1996); K.-P. Bell, S. A. Rice. J. Chem. Phys. **99** 4160 (1993); **104**, 1684 (1996).

[11] S. Karaborni, S. Toxvaerd, J. Chem. Phys. **96**, 5505 (1992); **97**, 5876 (1992); S. Karaborni, S. Toxvaerd, O. H. Olsen, J. Phys. Chem. **96**, 4965 (1992); S. Karaborni, Langmuir **9**, 1334 (1993); S. Karaborni, G. Verbist, Europhys. Lett. **27**, 467 (1996); J. I. Siepmann, S. Karaborni, M. L. Klein, J. Phys. Chem. **98**, 6675 (1994).

[12] M. Kreer, K. Kremer, K. Binder, J. Chem. Phys. **92**, 6195 (1990); M. Scheringer, R. Hilfer, K. Binder, J. Chem. Phys. **96**, 2269 (1991);

[13] Z. Cai, S.A. Rice, Faraday Discuss. Chem. Soc. **89**, 211 (1990); J. Chem. Phys. **96**, 6229 (1992); V. M. Kaganer, M. A. Opisov, I. R. Peterson, J. Chem. Phys. **98**, 3512 (1992); B. Pal, S. Modak, A. Datta, Surf. Science **310**, 407 (1993); S. M. Balashov, V. A. Krylov, Thin Solid Films **239**, 127 (1994).

[14] S. Opps, B. Yang, C. Gray, D. Sullivan, to be published.

[15] D. R. Swanson, R. J. Hardy, C. J. Eckhardt, J. Chem. Phys. **99**, 8194 (1993). M. D. Gibson, D. R. Swanson, C. J. Eckhardt, X. C. Zeng, J. Chem. Phys. **106**, 1961 (1997).

[16] S. W. Barton, A. Goudot, O. Bouloussa, F. Rondelez, B. Lin, F. Novak, A. Acero, S.A. Rice, J. Chem. Phys. **96**, 1343 (1992).

[17] F. Schmid, M. Schick, J. Chem. Phys. **102**, 2080 (1995); F. Schmid, Phys. Rev. E **55**, 5574 (1997).

[18] D. A. Pink, T. J. Green, D. Chapman, Biochemistry **19**, 349 (1980); A. Caillé, D. Pink, F. de Verteuil, M. Zuckermann, Can. J. de Physique **58**, 581 (1980).

[19] B. Dammann, H. C. Fogedby, J. H. Ipsen, C. Jeppesen, K. Jorgensen, O. G. Mouritsen, J. Risbo, M. C. Sabra, M. M. Sperotto, M. J. Zuckermann, Handbook of nonmedical applications of liposomes, Vol. 1, pp. 85 D. D. Lasic, Y. Barenholz eds., (CRC press, 1995).

[20] A. Ben-Shaul, I. Szleifer, W.M. Gelbart, J. Chem. Phys. **83**, 3597 (1985); 3612 (1985). I. Szleifer, A. Ben-Shaul, W.M. Gelbart, J. Chem. Phys. **85**, 5345 (1986).

[21] J. Harris, S. A. Rice, J. Chem. Phys. **88**, 1298 (1987); S. Shin, Z. Wang, S.A. Rice, J. Chem. Phys. **92**, 1427 (1989); **93**, 5247 (1990).

[22] M. Milik, J. Skolnick, A. Kolinski, J. Phys. Chem. **96**, 4015 (1992); Y.K. Levine, A. Kolinski, J. Skolnick, J. Chem. Phys. **98**, 7581 (1993);

[23] H. Stettin, H. J. Mögel, R. Friedemann, Ber. Bunsenges. Phys. Chem. **97**, 44 (1993); H. Stettin, H. J. Mögel, C. M. Care, Ber. Bunsenges. Phys. Chem. **100**, 20 (1996).

[24] F. M. Haas, P.-Y. Lai, K. Binder, Makromol. Chem. Theory Simul. **2**, 889 (1993).

[25] R. Hilfer, F. M. Haas, K. Binder, Nuovo Cimento **16**, 1297 (1994); F.M. Haas, R. Hilfer, K. Binder, J. Chem. Phys. **102**, 2960 (1995). F. M. Haas, R. Hilfer, K Binder, J. Phys. Chem. **100**, 15290 (1996).

[26] F. M. Haas, R. Hilfer, J. Chem. Phys. **105**, 3859 (1996).

[27] F. Schmid, C. Stadler, H. Lange, Computer Simulations in Condensed Matter Vol. 10, pp. 37, D. P. Landau, K. K. Mon, B. Schüttler eds. (Springer, 1997).

[28] H. Lange, Diplomarbeit Universität Mainz, 1996.

[29] C. Stadler, Dissertation Universität Mainz, 1998.

[30] F. Schmid, H. Lange, J. Chem. Phys. **106**, 3757 (1997).

[31] B. Fischer, E. Teer, C. M. Knobler, J. Chem. Phys. **103**, 2365 (1995); E. Teer, C. M. Knobler, C. Lautz, S. Wurlitzer, J. Kildae, T. M. Fischer, J. Chem. Phys. **106**, 1913 (1997).

[32] D.J. Rigby, R.J. Roe, J. Chem. Phys. **87**, 7285 (1987).

[33] C. Stadler, F. Schmid, in preparation.

[34] M. P. Allen, D. J. Tildesley, *Computer Simulation of Liquids*, (Oxford University Press, 1987).

[35] J. I. Siepmann, D. Frenkel, Mol. Phys. **75**, 59 (1992).

[36] B. I. Halperin, D. R. Nelson, Phys. Rev. Lett. **41**, 121 (1978).

[37] M. C. Shih, T. M. Bohanon, J. M. Mikrut, P. Zschack, P. Dutta, J. Chem. Phys. **96**, 1556 (1991).

[38] N. B. Wilding, A. D. Bruce, J. Phys. Cond. Matt. **4**, 3087 (1992).

[39] In fact, these studies were done for a slightly larger head size: $\sigma_H = 1.2\sigma$. For the liquid-gas transition, this should however not make much difference.

[40] The fact that the head groups have been modelled as purely repulsive units rather than Lennard-Jones beads does probably not make much difference. Adding an attractive part to the head interactions would certainly increase the probability of finding a liquid-gas transition, but presumably not affect the condensed phases very much. The main effect of the head beads in the condensed region is to put a restriction on the minimum grafting distance between molecules.

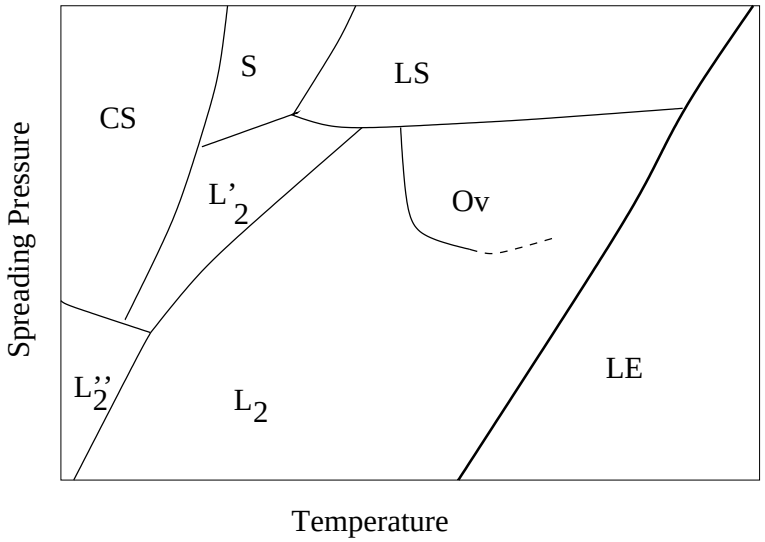

FIG. 1.

Generic phase diagram for fatty acid monolayers. The phases LS, S and CS are on average untilted, whereas Ov and L_2' show tilt towards next nearest neighbors, and L_2, L_2'' towards nearest neighbors. In CS, S, L_2' and L_2'', the backbones of the hydrocarbon chains are ordered. In CS and L_2'', the molecules have crystalline order in addition.

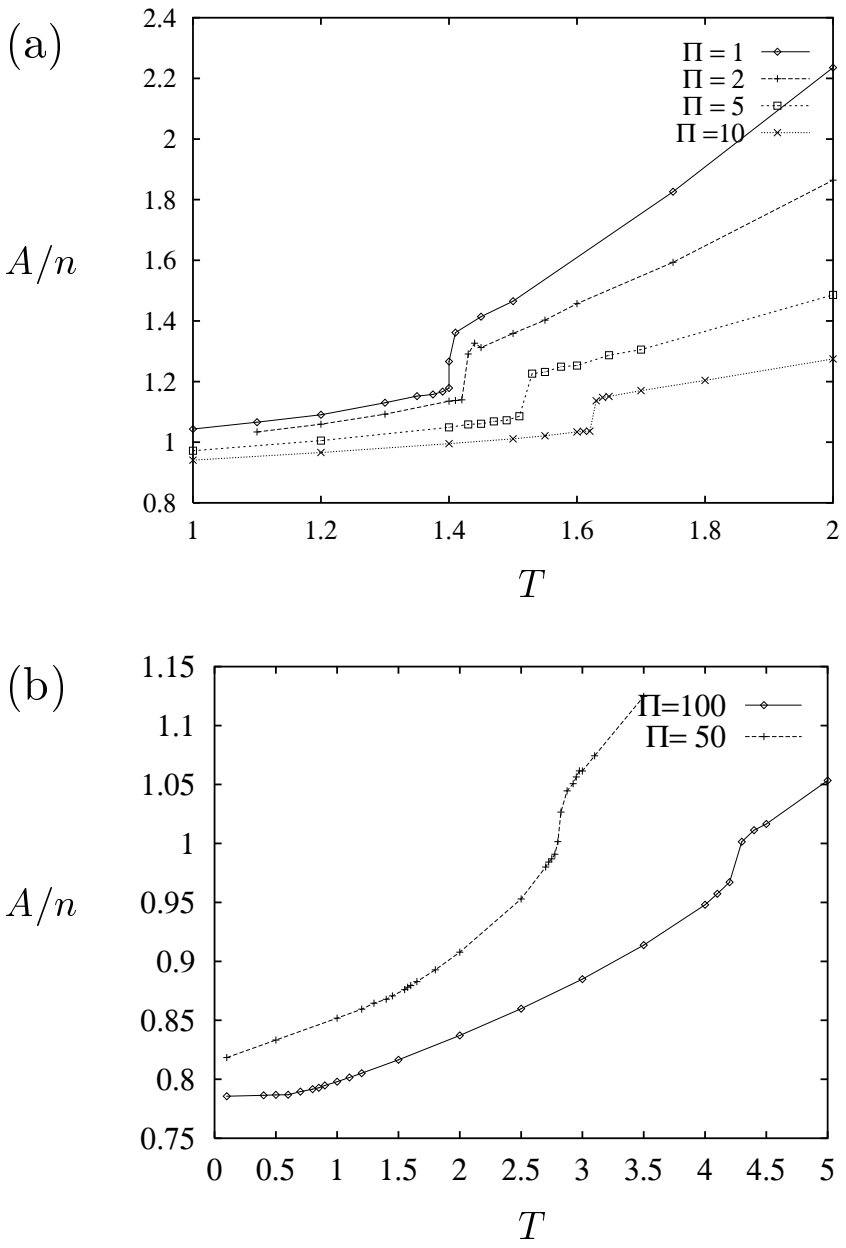

FIG. 2.

Area per molecule A/n in units of σ^2 vs. temperature T in units of ϵ/k_B for a choice of low (a) and high (b) pressures Π (in units of ϵ/σ^2) as indicated.

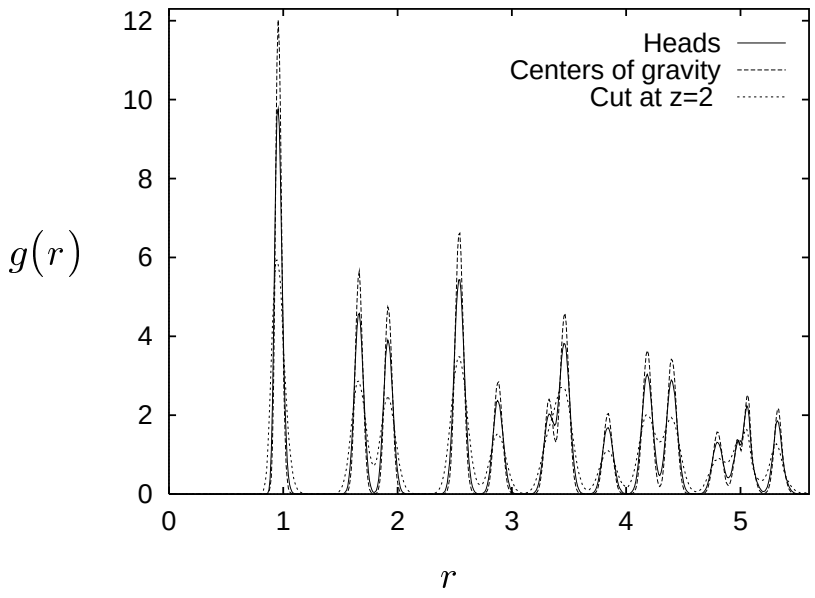

FIG. 3.

Radial pair correlation functions $g(r)$ vs. r in units of σ at pressure $\Pi = 100\epsilon/\sigma^2$ and temperature $T = 1\epsilon/k_B$. Correlation functions are shown for the heads (solid line), for the points where the molecules cross the plane at $z = 2\sigma$ above the surface (dotted line), and for the projection of the center of gravity onto the xy plane (dashed line). The values of $g(r)$ for $T = 0.1\epsilon/k_B$ are divided by a factor of five for the clarity of presentation.

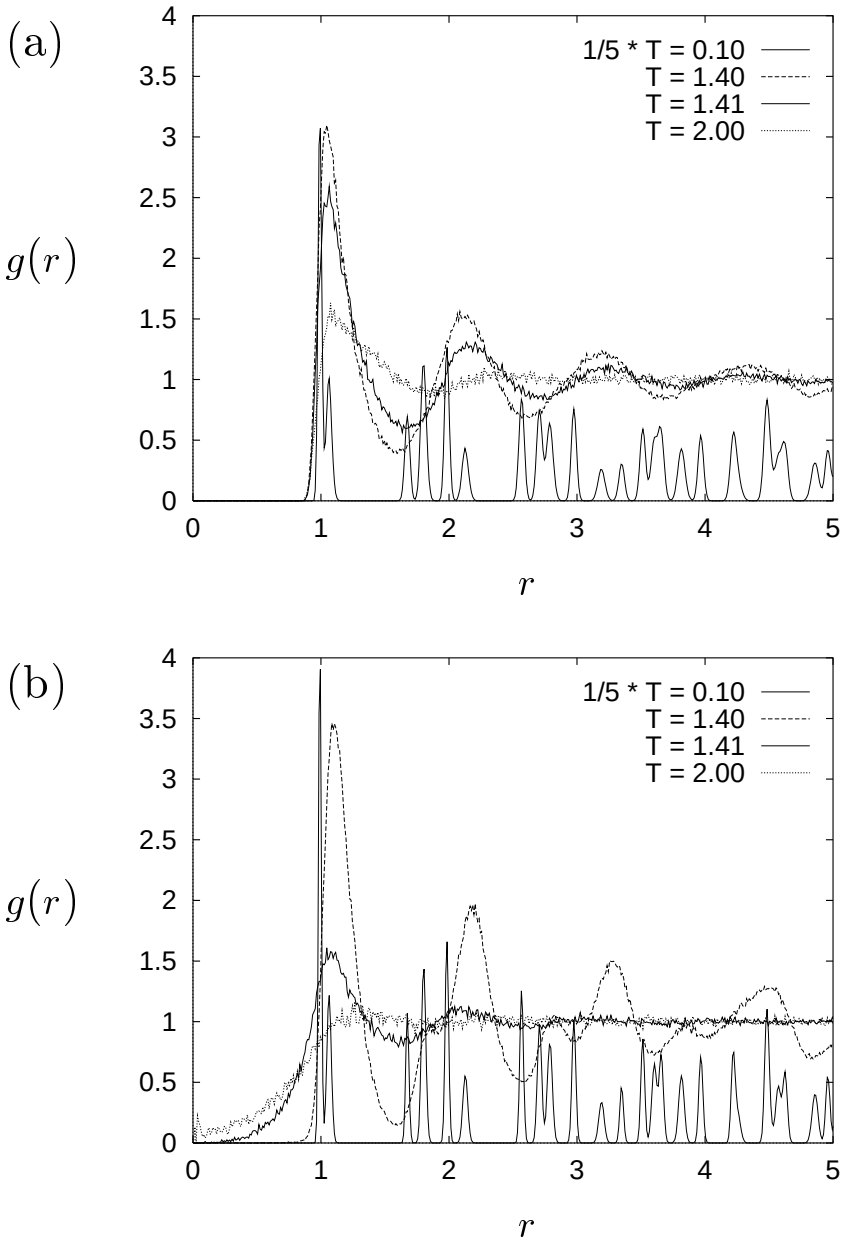

FIG. 4.

Radial pair correlation functions $g(r)$ vs. r in units of σ at pressure $\Pi = 1\epsilon/\sigma^2$ and various temperatures as indicated. Correlation functions are shown for the heads (a), and for projections into the xy plane of the centers of gravity (b). Temperatures T are given in units of ϵ. The correlation functions $g(r)$ for the temperature $T = 0.1\epsilon$ have been divided by a factor of 5.

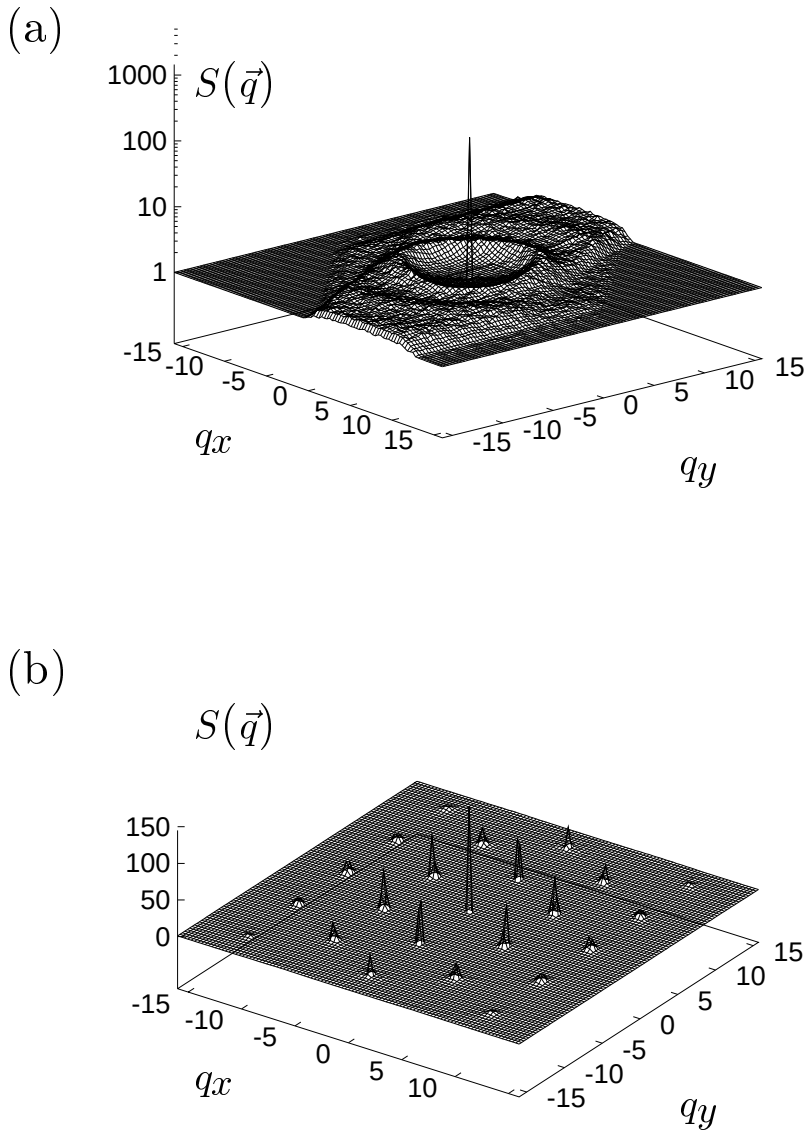

FIG. 5.

Structure factor $S(\vec{q})$ in the xy plane ($q_z = 0$) for a disordered state (a) and an untilted ordered state (b). Parameters are $\Pi = 10\epsilon/\sigma^2$, $T = 2.5\epsilon/k_B$ in (a), and $\Pi = 50\epsilon/\sigma^2$, $T = 2.0\epsilon/k_B$ in (b).

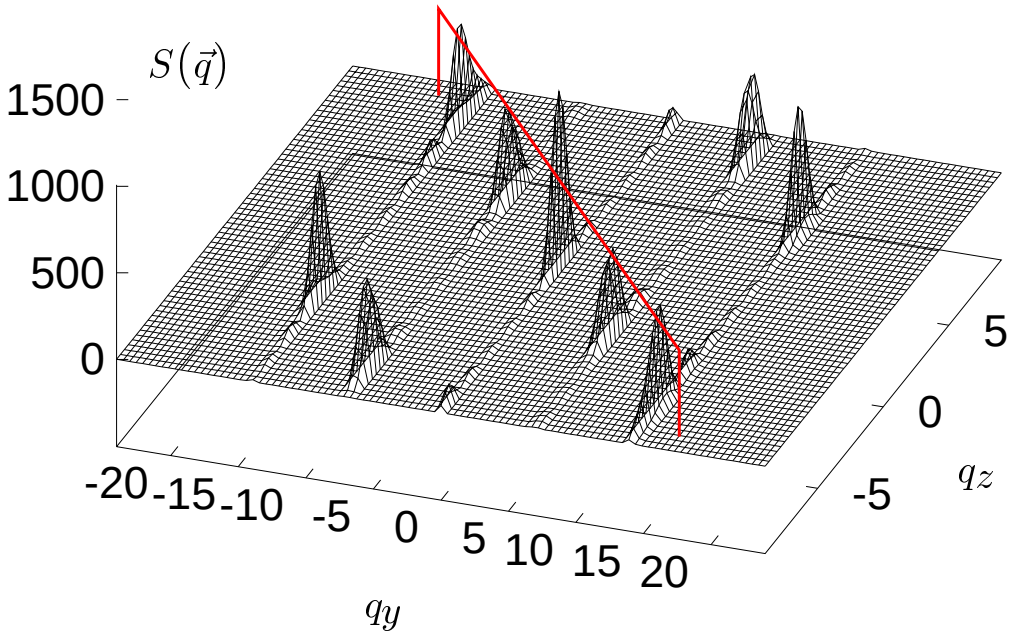

FIG. 6.

Structure factor $S(\vec{q})$ in the yz plane ($q_x = 0$) for an ordered state with tilt towards next nearest neighbors. Parameters are $\Pi = 50\epsilon/\sigma^2$ and $T = 0.1\epsilon/k_B$.

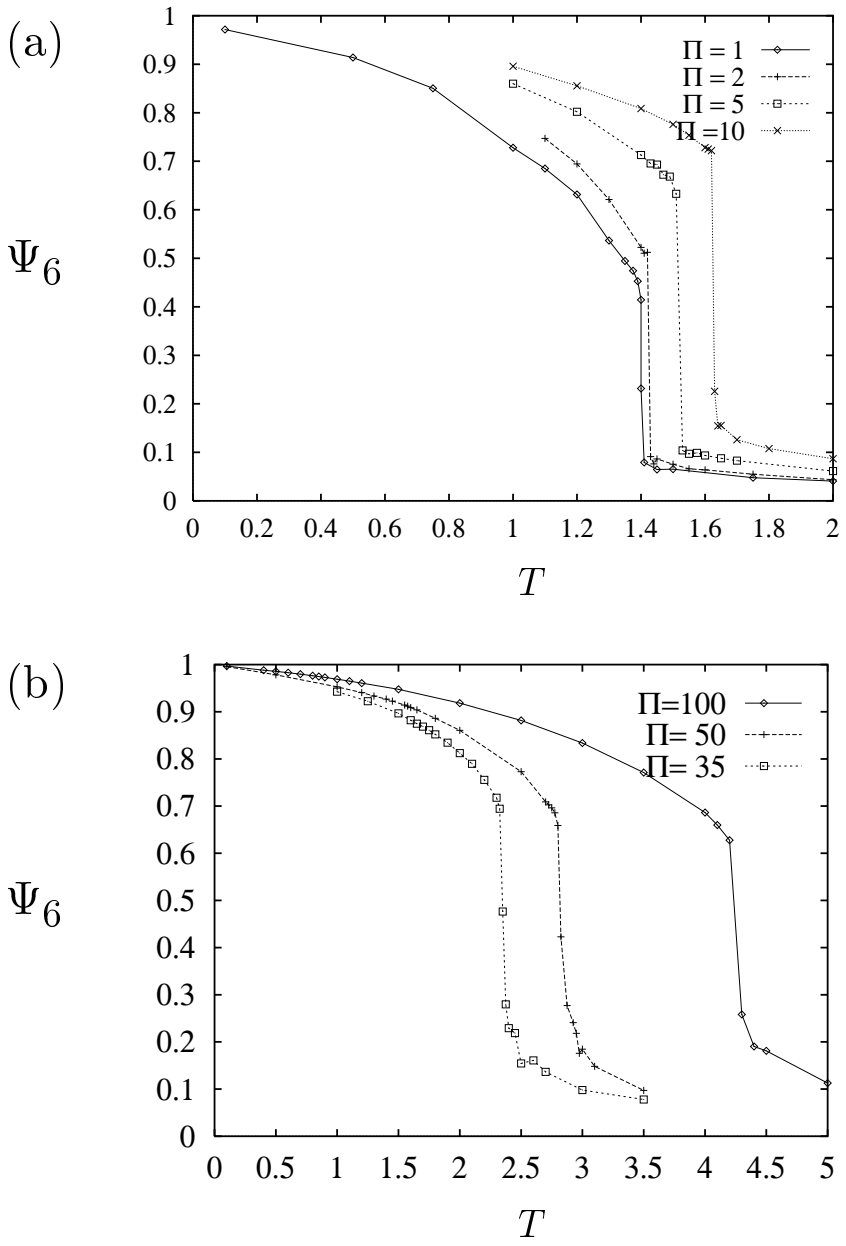

FIG. 7.

Order parameter Ψ_6 vs. temperature T in units of ϵ/k_B for different pressures Π (in units of ϵ/σ^2) as indicated.

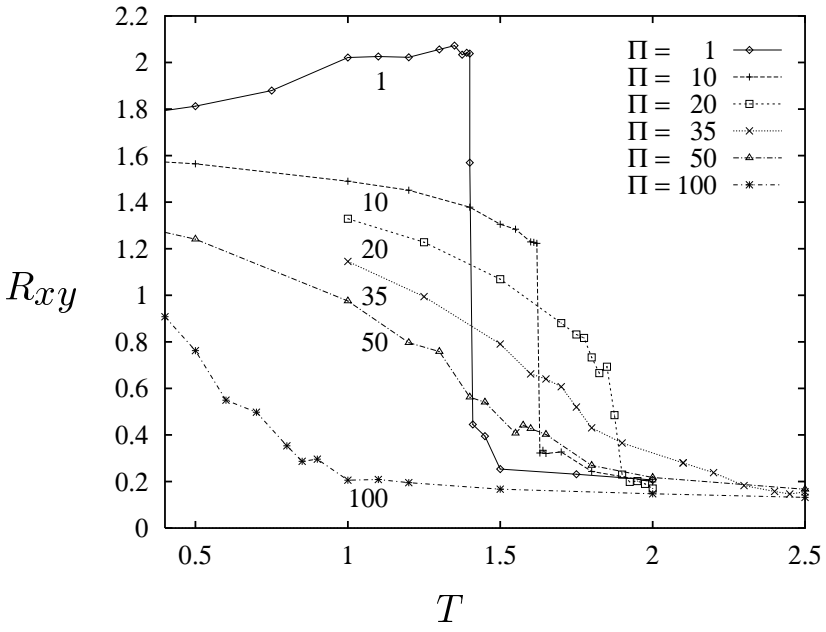

FIG. 8.

Order parameter R_{xy} in units of σ^2 vs. temperature T in units of ϵ/k_B for different pressures Π (in units of ϵ/σ^2) as indicated.

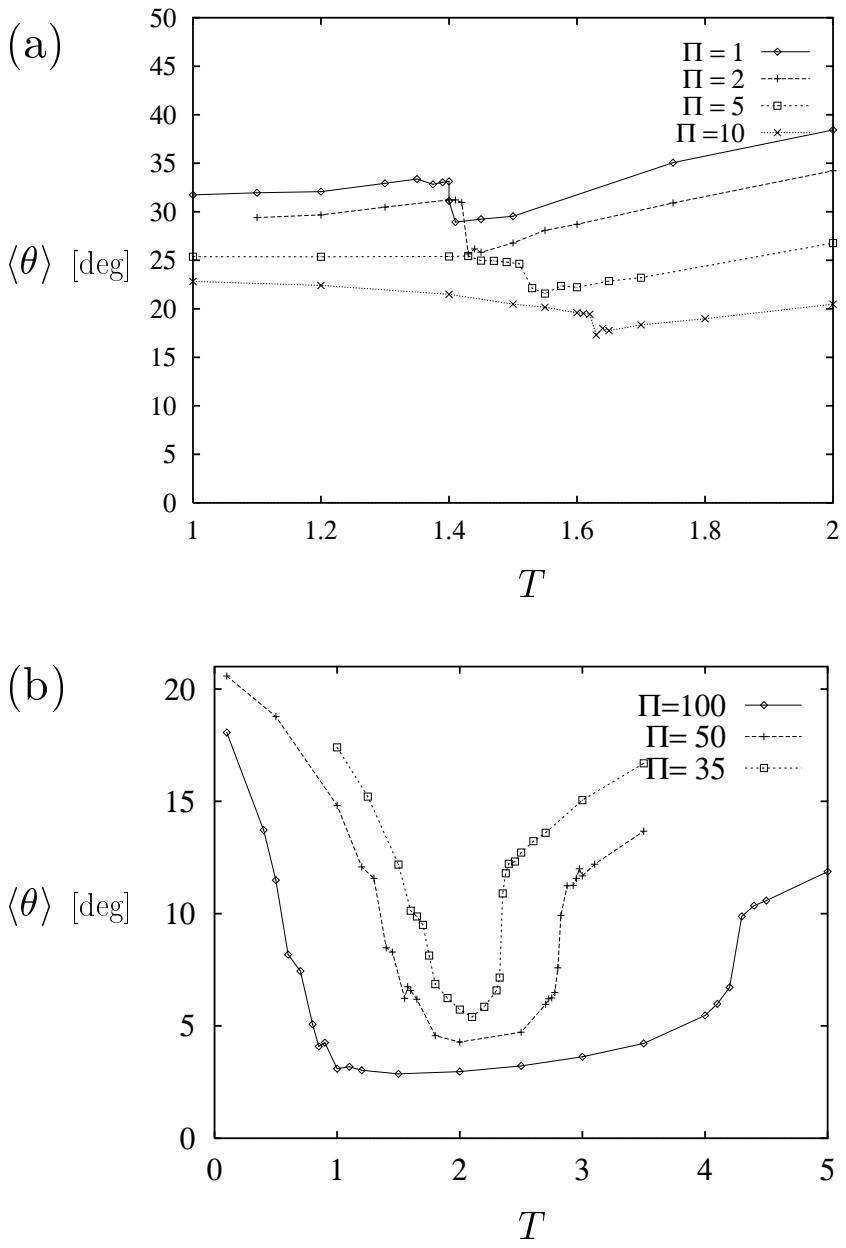

FIG. 9.

Average tilt angle $\langle\theta\rangle$ in degrees vs. temperature T in units of ϵ/k_B for different pressures Π (in units of ϵ/σ^2) as indicated.

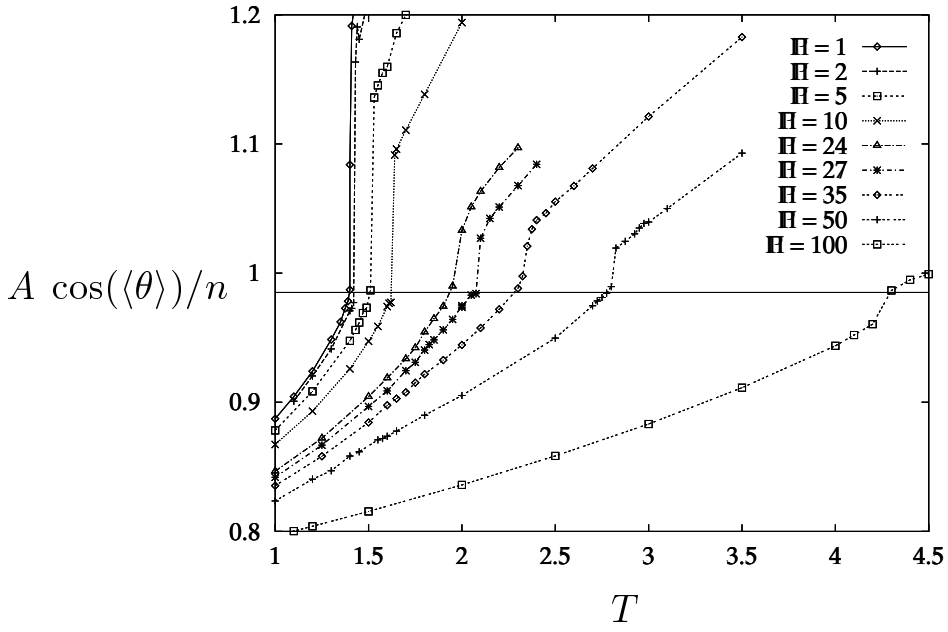

FIG. 10.

Product of the cosine of the average tilt angle with the area per molecule, $A\cos(\langle\theta\rangle)/n$, in units of σ^2, vs. temperature T in units of ϵ/k_B for different pressures Π (in units of ϵ/σ^2) as indicated. The horizontal line indicates the position of $a_c = 0.985\sigma^2$.

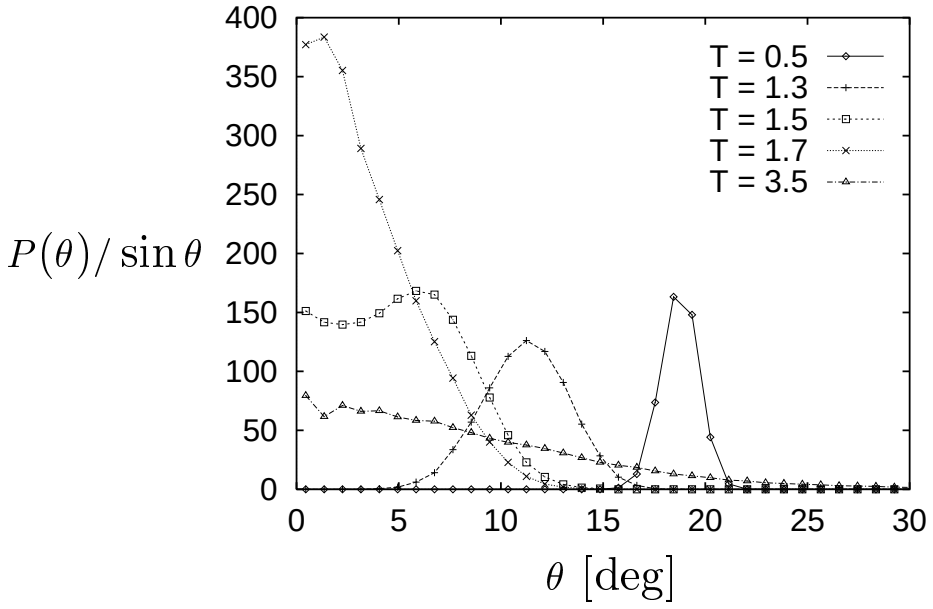

FIG. 11.

Histogram $P(\theta)/\sin\theta$ of the tilt angle θ (in degrees) at pressure $\Pi = 50\epsilon/\sigma^2$ for different temperatures (in units of ϵ/k_B).

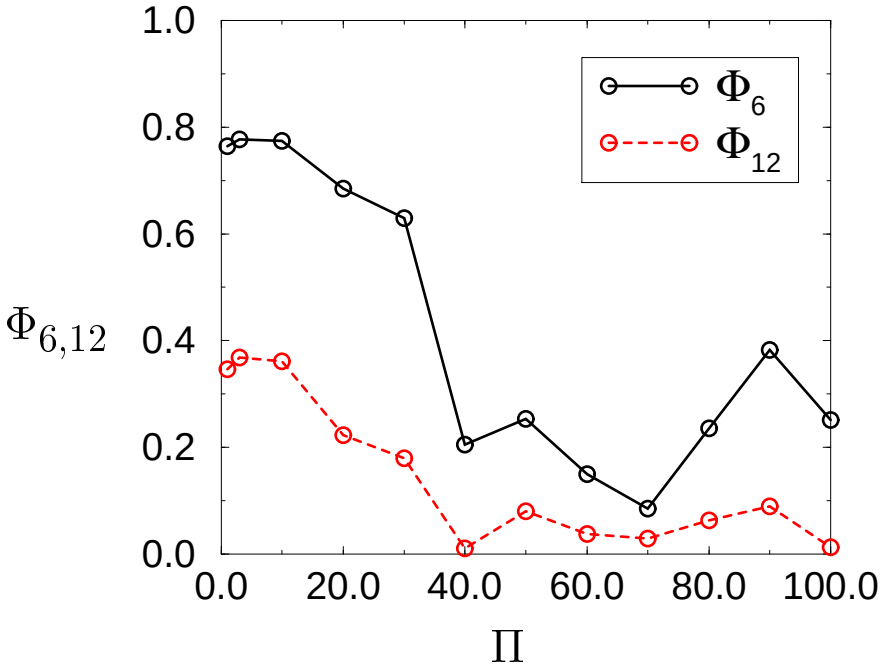

FIG. 12.

Order parameters Φ_6 and Φ_{12} vs. pressure Π in units of ϵ/σ^2 at temperature $T = 0.5\epsilon/k_B$.

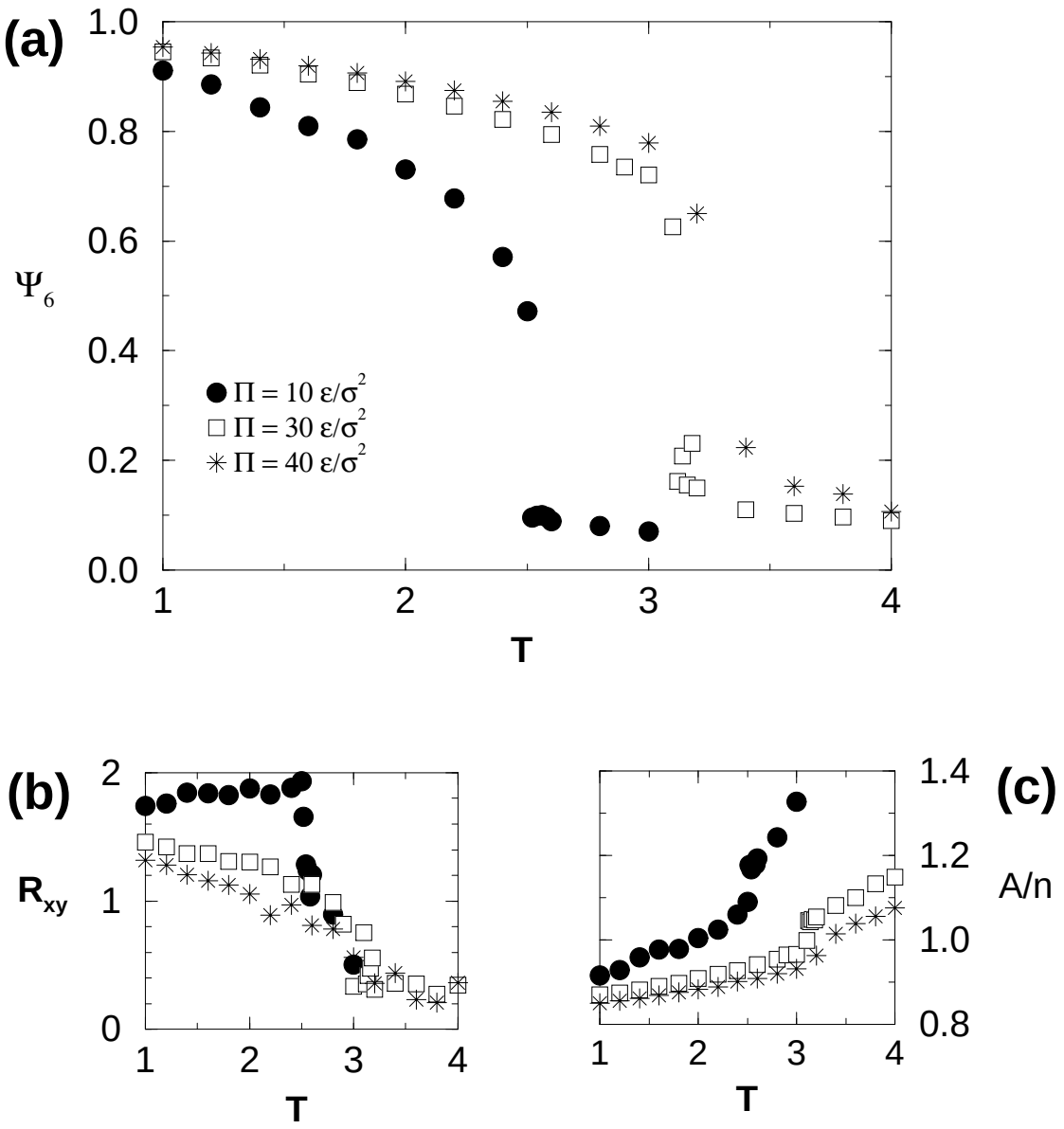

FIG. 13.

Order parameters Ψ_6 and R_{xy}, and area per molecule A/n vs. temperature T in units of ϵ/k_B for pressures $\Pi = 10\epsilon/\sigma^2$ (filled circles), $30\epsilon/\sigma^2$ (open squares), $40\epsilon/\sigma^2$ (stars) in systems of stiff chains, ($k_A = 100\epsilon$).

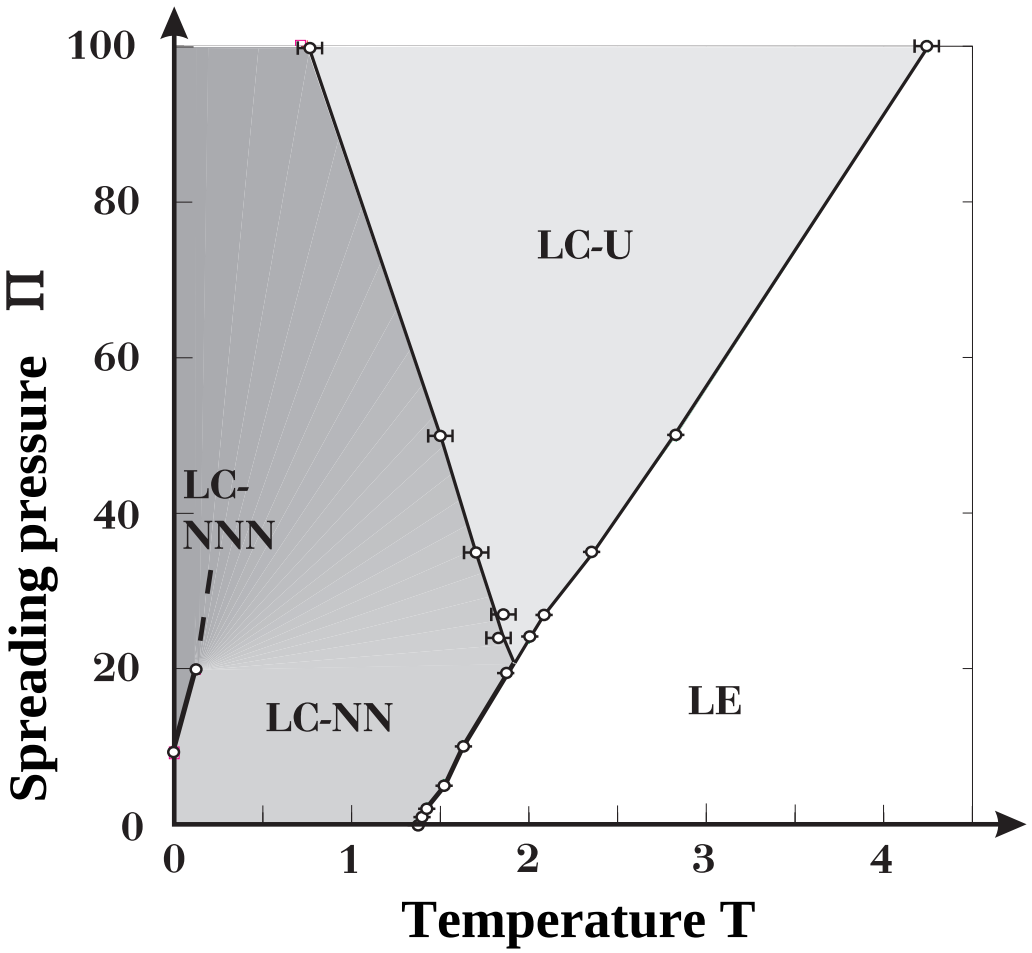

FIG. 14.

Phase diagram in the pressure-temperature plane. Pressure Π is given in units of ϵ/σ^2, and temperature T in units of ϵ/k_B. LE denotes disordered phase, LC-NN ordered phase with tilt towards nearest neighbors, LC-NNN ordered phase with tilt towards next nearest neighbors, and LC-U untilted ordered phase. The transition between LC-NN and LC-NNN could not be located at pressures above $\Pi = 20\epsilon/\sigma^2$. See text for more explanation.

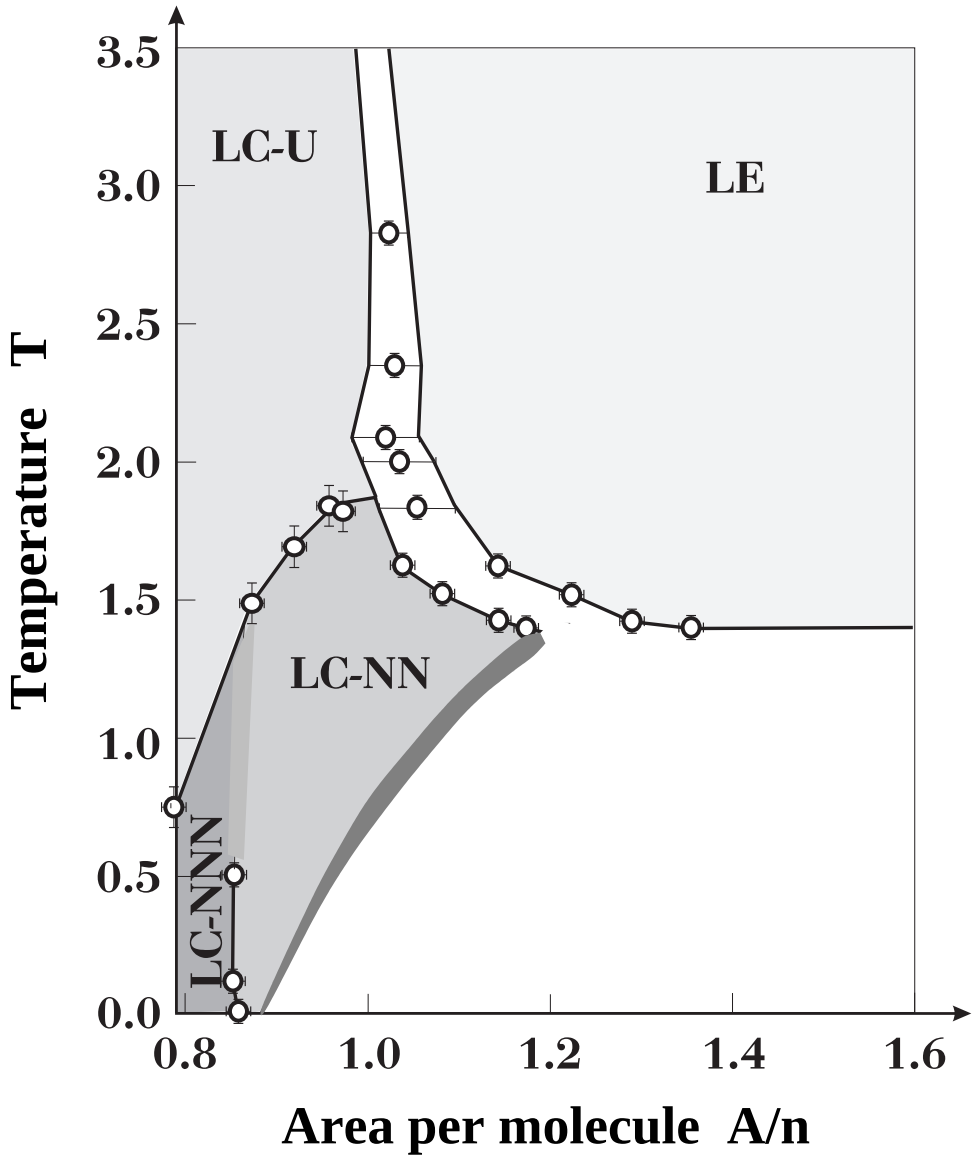

FIG. 15.

Phase diagram in the area-temperature plane. Area per molecule A/n is given in units of σ^2, and temperature T in units of ϵ/k_B. LE denotes disordered phase, LC-NN ordered phase with tilt towards nearest neighbors, LC-NNN ordered phase with tilt towards next nearest neighbors, and LC-U untilted ordered phase. See text for more explanation.